Probing Porous Polymer Resins by High-Field Electron Spin Resonance Spectroscopy

D. Leporini,[†,‡] X. X. Zhu,[*,§] M. Krause,[§] G. Jeschke,[†] and H. W. Spiess[*,†]

Max Planck Institut für Polymerforschung, Postfach 3148, D-55021 Mainz, Germany; Dipartimento di Fisica "Enrico Fermi", Universita' di Pisa, V.F.Buonarroti 2, I-56127 Pisa and INFM, UdR Pisa, Italy; and Département de chimie, Université de Montréal, C.P. 6128, succursale Centre-ville, Montreal, QC, H3C 3J7 Canada

Received October 25, 2001

ABSTRACT: High-field W-band (95 GHz) electron spin resonance spectroscopy of various spin probes was used to study the structure of highly cross-linked porous polymer resins based on a styrene−divinylbenzene matrix. The pores of these resins were created by template imprinting with reverse micelles solubilized in the mixture of monomers and cross-linkers prior to the polymerization. Functional groups in the resins were introduced by the use of polymerizable cosurfactants in the reverse micelles. Sufficiently large unpolar spin probes exhibit a distribution of mobilities that can be attributed to regions with different degrees of cross-linking in the polymer. The dynamics of a surfactant spin probe is sensitive to the presence of pores and the functionalization of the pore surface with highly polar groups. This effect disappears when the headgroup of the surfactant spin probe is esterified. It can be considered as a structural memory effect related to the use of reverse micelles as templates for imprinting. The result indicates that the pores can be filled or washed selectively.

Introduction

Selective interactions of molecules or molecular aggregates according to their size and shape are important for self-assembly of materials by supramolecular interactions and for improved controls of chemical processes.[1] Polymer materials with well-defined porous structures can serve the latter purpose and are thus useful in various applications such as chemical catalysis[2] and selective binding and removal of drugs[3,4] and biological molecules such as proteins[5,6] and nucleotide bases.[7] The preparation of cross-linked synthetic polymers with size- and shape-specific binding sites is usually achieved by template-imprinting techniques.[8−10] Recently, molecular aggregates such as reverse micelles have been found to be suitable templates for imprinting polymer resins with cavities of specific sizes.[11−14] This control of the pore size is achieved in a very simple fashion, as the size of the reverse micelles formed by sodium bis(2-ethylhexyl) sulfosuccinate (AOT) can be controlled by varying the water content inside.

The further development of such materials, in particular their fine-tuning, requires advances in structural characterization. While the size of the pores in the dry state can be measured by BET gas absorption−desorption experiments, the accessibility of these pores by molecules of different sizes cannot be easily monitored. To date, the method of choice for the latter purpose is liquid chromatographic tests with molecules of different sizes, but these can only provide indirect information.[15] Direct information could be obtained by tracer techniques. Among these, electron spin resonance (ESR) spectroscopy appears to be particularly well suited, since a multitude of ESR tracers (spin probes) with different size, shape, and polarity are readily available. Furthermore, the spectral line shapes of the spin probes depend strongly on their rotational dynamics, and the interpretation of probe dynamics in relation to structure and dynamics of the matrix is established for various materials of current interest, such as biological samples, liquid crystals, polymers, and liquids in normal or supercooled states.[16−24] Specific characterization of sections of a polymer chain[18,25] or domains in complex systems[26−28] have been demonstrated. Hydrogen-bonded spin probes can also be attached to specific sites in a polymer.[29] In suitable cases their dynamics scales with the polymer relaxation.[30] The interaction of a variety of surfactant spin probes with different classes of polymers has been investigated in some detail by several groups.[31−34] In many of these experiments the spin probe is not chemically attached to the host molecule but is accommodated in the available free volume. Thus, it appears to be quite natural to use an ESR spin probe approach to characterize porous materials. The versatility of such studies is enhanced by recent technical advances, which made possible the detection of continuous wave (CW) ESR signals at W band (95 GHz) and high magnetic fields $B_0 = 3.4$ T.[35] This leads to increased spectral resolution and enhanced orientation selectivity, which in turn allow for the detection of quite subtle differences in the rotational dynamics of the spin probes.[36,37] It remains to be explored whether such slight differences in probe dynamics can be used to extract reliable information on polymer structure and on the interaction between additives and polymers. The present work answers this question by applying high-field ESR measurements on spin probes to sense the presence and functionalization of nanosized pores in new porous polymer resins.[13−15]

Experimental Section

Sample Preparation. The polymer resins were prepared by bulk copolymerization of styrene (S) and divinylbenzene (DVB) as described previously.[13] To create the porous structure, the polymer resins were template-imprinted with reverse

* To whom correspondence should be addressed: e-mail julian.zhu@umontreal.ca, spiess@mpip-mainz.mpg.de.
† Max Planck Institut für Polymerforschung.
‡ Universita' di Pisa.
§ Université de Montréal.

10.1021/ma011861a CCC: $22.00
Published on Web 04/16/2002

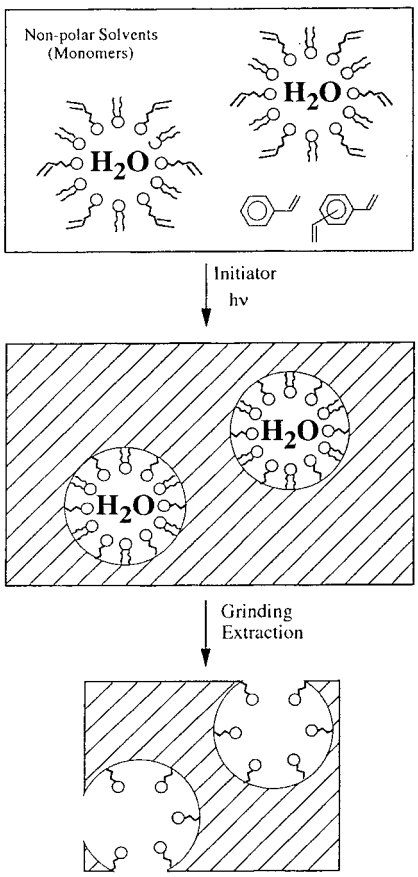

Figure 1. Preparation scheme of the polymer resins. The pore size can be controlled by adjusting the water content inside the reverese micelles prior to polymerization. The functionalization of the pore surface is achieved by admixing polymerizable surfactants.

micelles of sodium bis(2-ethylhexyl) sulfosuccinate (AOT), which was dissolved in the mixture of comonomers prior to the initiation of the polymerization (Figure 1). The pore size can be adjusted by the amount of water contained in the reverse micelles. BET sorption and desorption with nitrogen were used for the characterization of the porous resins in the dry state.[13,14] The factors affecting the porosity of the resin were studied and optimized.[14] AOT was dissolved in the mixture of the comonomers at a concentration of 0.2 M. For the porous samples used in this work, the water-to-AOT molar ratio (W) in the reverse micelles was fixed at 12. The amount of the cross-linker (DVB) used was set at 50 vol %, but the purity of DVB was 55%, which means that the actual degree of cross-linking is ca. 27.5%. Bulk polymerization was initiated upon the addition of 2 wt % of AIBN followed by ultraviolet (UV) irradiation at a wavelength of 254 nm. The resulting resin (RW12) was subsequently ground and washed in a Soxhlet extractor (starting with toluene, changed into ethanol, then water, then ethanol, and final diethyl ether). It was then dried above 373 K for at least 1 day and sieved. The fraction with particle size <120 mesh (less than 125 μm in diameter) was used in the inverse size exclusion chromatography.[15] The heating cycle resulted in no weight change or changes in the porous structure. Solvent removal was complete as evidenced by NMR.[14] The resin without imprints (RW0) was synthesized under the same conditions with the same degree of cross-linking but without the AOT reverse micelles. Hydroxyl and sulfonic acid groups were introduced into the resin cavities by the use of polymerizable cosurfactants (see Figure 1) such as 2-hydroxylethyl methacrylate and sodium styrenesulfonate (both purchased from Aldrich). Henceforth, the functionalized porous resins will be denoted as RW12-OH and RW12-SO_3^-. The amount of the polymerizable cosurfactant was ca. 40 mol % of the amount of AOT dissolved in the mixture of the comonomers. These highly cross-linked polymers exhibit no glass transition up to their decomposition temperature above 570 K.[13,14] They are less susceptible to effects of thermal history than linear polymers.

The ESR spin probes TEMPO, 7-DOXYL-stearic acid (SA) and its methyl ester (ME), 3-DOXYL-17β-hydroxy-5α-androstane (AN), and 3β-DOXYL-5α-cholestane (CH) were all purchased from Aldrich and used without further purification. Their chemical structures are shown in Figure 2. The spin probes were dissolved in methanol (1 mM), and 1 mL of the solution was mixed with 100 mg of each polymer resin and stirred for 3 days. A first group of samples was obtained by drying the resins at about 380 K for at least 1 day under vacuum and transferred to capillary tubes (0.7 mm i.d.) for the ESR measurements. This class of samples are referred to as "unwashed" samples. Alternatively, after stirring the solution, the latter was filtered off, and the resins were washed with dichloromethane for 2 h. Then, the solvent was filtered, and the resin was rinsed and also dried at about 380 K for at least 1 day under vacuum. These samples will be referred to as "washed" samples. No segregation of the spin probes in both washed and unwashed samples was evidenced in the ESR spectra. No residual solvents were detected by NMR.

ESR Spectroscopy. The CW ESR experiments were carried out on a Bruker E680 spectrometer operating at 95 GHz (W band) with a Bruker Teraflex probehead. All spectra were recorded at room temperature and stored in a computer for off-line analysis**.** For the simulation of the line shapes we used numerical routines described elsewhere.[38,39] Alternative software is available.[40] The routines were originally developed for X-band line shapes and now extended to the W-band case by taking into account the nuclear Zeeman interaction. The evaluation assumes that the reorientation occurs after a mean residence time τ in each orientation by sudden jumps of angular width ϵ_0 around isotropically distributed rotation axis.[30,41] The corresponding rotational correlation time τ_2 (the area below the correlation function of the spherical harmonic $Y_{2,0}$) is $\tau/[1 - \sin(5\epsilon_0/2)/(5\sin(\epsilon_0/2))]$. In addition to the rotational model parameters the other input parameters to calculate the ESR line shape are the principal components (g_x, g_y, g_z) and (A_x, A_y, A_z) of the electron **g** tensor and the hyperfine tensor, respectively. The x axis of the principal frame for both tensors is parallel to the N−O bond, the z axis is parallel to the nitrogen and oxygen 2π orbitals containing the unpaired electron, and the y axis is perpendicular to the xz plane (Figure 2). For each spin probe the components are determined by fitting the corresponding rigid-limit powder line shape and are fixed during the fitting of the spectra of mobile probes.

Results and Discussion

ESR Line Shapes and Molecular Motion. The W-band ESR line shapes change markedly for rotational motions on time scales between tens of picoseconds and tens of nanoseconds as summarized by the numerical simulations which are shown in Figure 3. The main broadening mechanism of the ESR line shape is the coupling between the reorientation of the spin probe and the relaxation of the electron magnetization M via the anisotropy of the electron Zeeman and the hyperfine magnetic interactions. When the molecule rotates, the coupling gives rise to fluctuating magnetic fields acting on the spin system. The resulting phase shifts and transitions relax the magnetization and broaden the resonance. For reorientation that is much faster than the ESR time scale ($\tau_2 = 66$ ps), the anisotropy of the interactions is averaged, and a triplet of fairly narrow lines is observed (fast limit, Figure 3a). The splitting is due to the hyperfine coupling to the ^{14}N nucleus and the widths of the three lines due to hyperfine-dependent relaxation rates. For slower reorientation ($\tau_2 = 460$ ps), these line width differences become more pronounced, and the clearly discernible triplet structure is lost

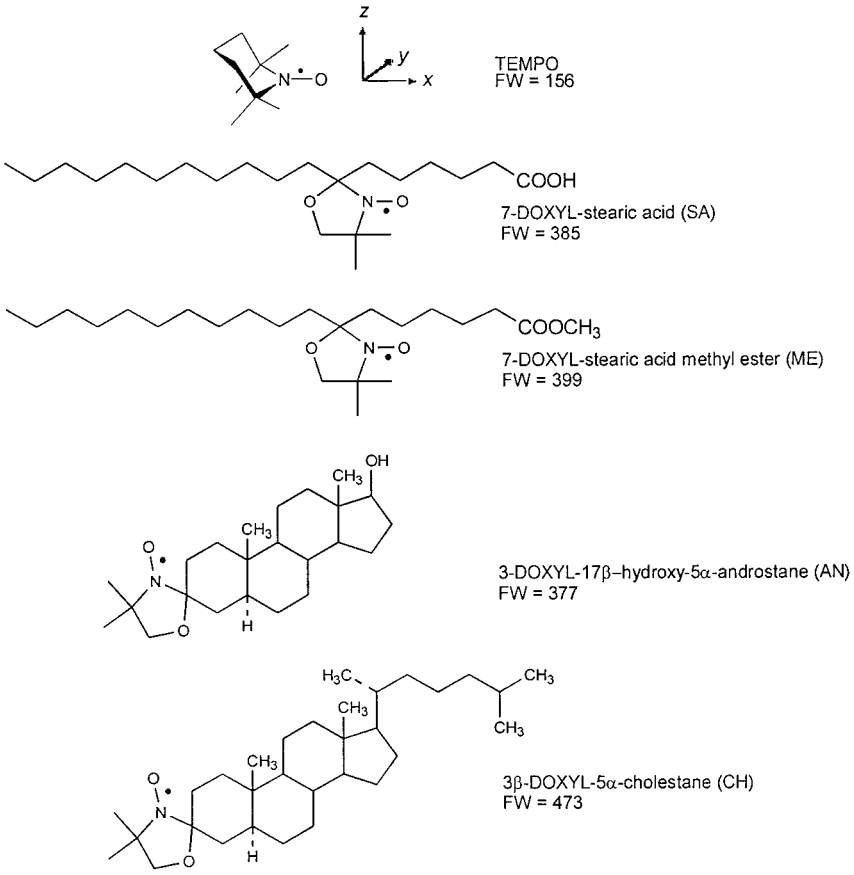

Figure 2. Molecular structure of the spin probes used and definition of the principal axes frames of the **g** and hyperfine tensor.

(transition to slow tumbling, Figure 3b). When the reorientation rate decreases further, the spectrum becomes significantly broader, as the anisotropy of the **g** and hyperfine tensors is no longer averaged (slow tumbling, Figure 3c). In the slow tumbling regime with correlation times (τ_2) between approximately 0.5 and 20 ns, the line shape is most sensitive to the rate and specifics of the reorientation process. Finally, when the motion becomes significantly slower than the time scale of the CW ESR experiment, the line shape can be hardly distinguished from the line shape in the rigid limit ($\tau_2 > 50$ ns, transition to rigid limit, Figure 3d).

The dynamics of spin probes in polymers is affected by polymer motion to a degree which strongly relies on the coupling strength.[18] Recently, the scaling between the polymer relaxation and the dynamics of spin probes which can form hydrogen bonds or ionic structures was evidenced.[26,30] In the present work, we therefore tune the coupling strength by variation of the size and functionality of the spin probes.

Classification of ESR Line Shapes. For the spin probe TEMPO, the ESR line shape was found to be virtually the same for all the resins under investigation. This was ascribed to the small size of this radical, which is insufficient to probe the structural features of interest. Therefore, all further discussions will be limited to the larger AN, CH, SA, and ME spin probes (Figure 2).

Despite the wide variety of resins and spin probes under study, the ESR line shapes may be grouped in terms of three typical patterns. As an illustration, their numerical simulations are shown in Figure 4. Two patterns are typical of spin probes which are either exclusively fast reorienting (F-type) or exclusively slowly reorienting (S-type). The F-type motion is not rapid enough to completely average the anisotropic spin interactions as shown in Figure 3a. Instead, a single relatively broad resonance, corresponding to an intermediate case between parts b and c of Figure 3, is observed (e.g., see the line shape with $\tau_2 = 1.61$ ns in Figure 4). The S-type line shape resembles that of Figure 3d. The third line shape is a weighted sum of the S- and F-types (SF-type) and indicates a bimodal distribution of mobilities. It is shown here for two different fractions of the fast component ($w_f = 0.7$ and $w_f = 0.3$). Table 1 summarizes the results of the above basic classification for the different spin probes and samples studied. Differences between SF-type line shapes of the same probe in different polymers will be discussed below. No spectrum was obtained for the CH probe in washed samples of RW0, which indicates that this probe is completely removed from the nonporous polymer by the washing process. It is somewhat unusual that the probe AN of a similar molecular size exhibits a slightly higher affinity to the polymer resin, probably due to the absence of the hydroxyl group in this probe.

Effects of Probe and Solvent Polarity. For the probes AN and ME the washing process leads to changes in the distribution of the rotational correlation times already in the nonporous resin (see probe AN in Figure 5). We tentatively assign this effect to the different distributions of these unpolar spin probes in the polymer resins suspended in the more polar methanol ($\epsilon = 33.0$) and the less polar dichloromethane ($\epsilon = 8.93$). In methanol suspensions, these unpolar spin probes are expected to prefer sites in the most densely cross-linked regions, as these cannot as easily be swollen and contain a smaller fraction of the polar solvent. After drying, the spin probes are thus effectively immobilized

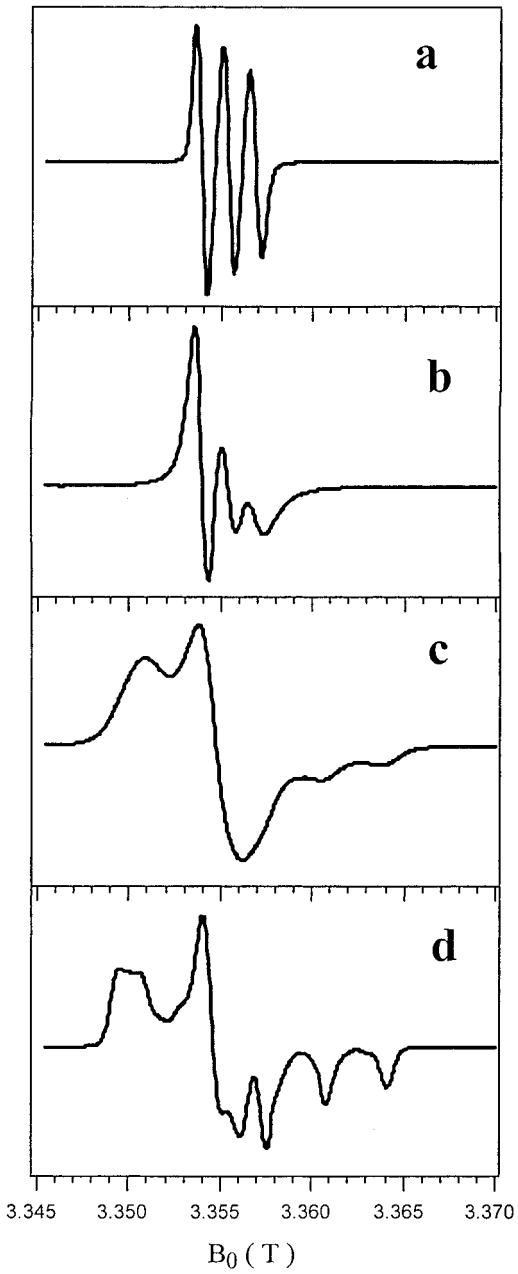

Figure 3. Dependence of the ESR line shape on the rotational correlation time of the spin probe τ_2 (simulations). The spin probes are assumed to rotate by jumps of size $\epsilon_0 = 60°$ with a rotational correlation time τ_2. The **g** tensor principal values are $g_x = 2.0093$, $g_y = 2.0063$, and $g_z = 2.0028$, and the hyperfine tensor principal values are $A_x = 19.61$ MHz, $A_y = 14.01$ MHz, and $A_z = 90.06$ MHz. All line shapes were convoluted with a Gaussian curve with a variance of 0.2 mT. (a) Fast limit, $\tau_2 =$ 66 ps. (b) Transition to slow tumbling, $\tau_2 = 460$ ps. (c) Slow tumbling, $\tau_2 = 6.6$ ns. (d) Close to the rigid limit, $\tau_2 = 46$ ns.

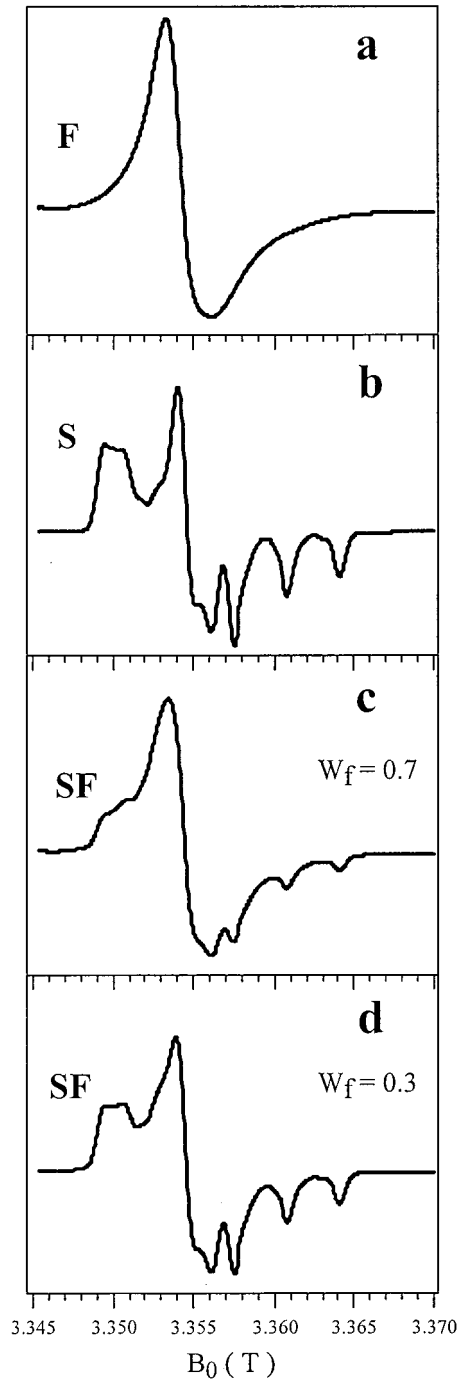

Figure 4. Three typical patterns of the ESR spectra (simulations). The line shapes correspond to jump size $\epsilon_0 = 60°$ and rotational correlation times $\tau_2 = 1.61$ ns (F pattern) and 46 ns (S pattern). The SF pattern is a weighted superposition of the S and F line shapes. Magnetic and convolution parameters are as in Figure 3.

and exhibit only the S-type spectrum. In dichloromethane suspensions, on the other hand, the differences in the polarity of the densely cross-linked and less cross-linked regions are smaller. The unpolar spin probes may thus distribute between both types of sites and exhibit SF-type spectra. In this picture, the F-type spectrum of the SA probe with its polar headgroup also finds a natural explanation, since the headgroup is expected to prefer the most polar sites. These sites are in the less cross-linked regions, where the concentration of the polar solvent is higher. In agreement with this preference for the solvent over the polymer, a significant part of the SA probes is removed from the nonporous sample RW0 by washing. Note also that the existence of a small fraction of slowly reorienting SA probes (<10%) cannot be excluded by our simulations given the limited signal-to-noise ratio in the spectra.

The S-type spectra of AN, CH, and ME in both nonporous and porous unwashed samples can best be simulated by assuming that the nitroxide moieties of these probes undergo reorientations by large-angle jumps with $\epsilon_0 = 60°$.[30,38,39] Such large-angle reorientation was already reported for doxyl stearic acids and esters in polymer aggregates.[34] As an example, the

Table 1. Basic Classification of the ESR Line Shapes of the Spin Probes Mixed in the Different Resins before and after Washing[a]

	RW0		RW12		RW12-OH		RW12-SO_3^-	
probe	without washing	with washing	without washing	with washing	without washing	with washing	without washing	with washing
AN	S	SF	S	SF	S	SF	S	SF
CH	S		S	SF	S	SF	S	SF
ME	S	SF	S	SF	S	SF	S	SF
SA	F	F	F	SF	F	SF	F	SF

[a] For a quantification of differences between SF line shapes in different polymers, see Table 2. See text for details. Note: S and F indicate slow and fast components, respectively.

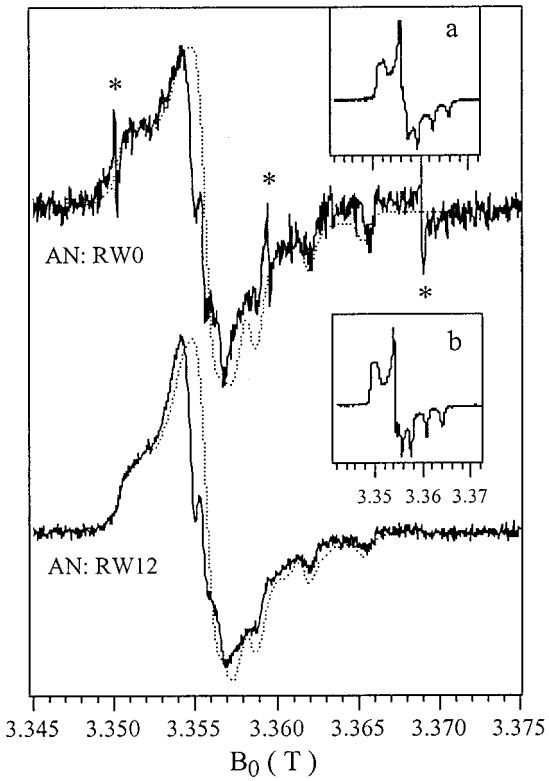

Figure 5. Experimental ESR line shapes of AN in RW0 and RW12 resins after washing. The insets refer to RW0 (a) and RW12 (b) resins before washing. The superimposed dotted lines are the simulated line shapes being expressed as a weighted sum of two components: one F-component ($\tau_2 = 2.0$ ns) and one S-component ($\tau_2 = 46$ ns). The weight fractions are $w_s = 0.4$, $w_f = 0.6$ for RW0 and $w_s = 0.3$, $w_f = 0.7$ for RW12 resins. All the other parameters are as in Figure 3. The narrow peaks marked by asterisks in the upper traces are signals due to manganese impurities.

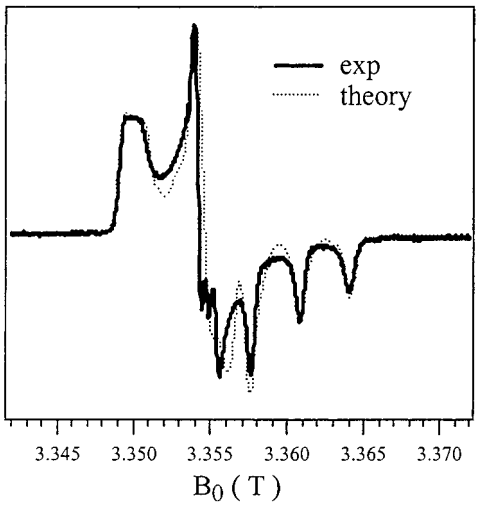

Figure 6. Comparison of the experimental ESR line shape of the AN spin probe in unwashed RW12 resin with a simulated line shape assuming the jump model with $\epsilon_0 = 60°$ and $\tau_2 = 46$ ns. Magnetic and convolution parameters are as in Figure 3.

Table 2. Fractions of the Slow Component (w_s) of the SF-Type ESR Line Shapes of the Spin Probes Mixed in the Washed Resins[a]

probe	RW0	RW12	RW12-OH	RW12-SO_3^-
AN	0.4	0.3	0.2	0.2
CH		0.3	0.3	0.3
ME	0.3	0.3	0.3	0.3
SA	0.0	0.3	0.3	0.6

[a] See text for details.

experimental and simulated ESR line shapes of AN in unwashed RW12 are shown in Figure 6. The experimental and simulated spectra agree quite well. The reorientation of AN, CH, and ME in unwashed samples exhibits correlation times of about 50 ns. On this time scale, the broadening of the ESR line shape has limited sensitivity to the rotational dynamics. This prevents the detailed characterization of the reorientation process. Nonetheless, we found that, if the jump size ϵ_0 is decreased to approach the small-angle diffusion limit, the quality of the fit becomes worse. In particular, the discrepancies are not recovered by considering anisotropic diffusion due to the prolate shape of AN, CH, and ME. This finding agrees with the conclusion of another ESR study on the reorientation of CH in the glass-former *o*-terphenyl.[41]

The SF-type spectra of AN, CH, and ME in washed samples again do not exhibit significant differences for nonporous, porous unfunctionalized, and porous functionalized samples (see Table 2). For example, all the spectra for AN can be simulated by a superposition of 20% of an S-type spectrum with a rotational correlation time of 46 ns and 80% of an F-type spectrum with a rotational correlation time of 2 ns. Jump reorientation with $\epsilon_0 = 60°$ is assumed in both cases. The insensitivity of the unpolar spin probes to the presence and functionalization of pores is not surprising, since the above discussion suggests that they prefer the polymer bulk. These spin probes may thus only be suitable to characterize the specifics of cross-linking.

Structural Memory Effect for Surfactant Probes. In contrast, the spectra of SA in washed samples depend significantly on the presence of pores and on their functionalization, as can be seen in Figure 7. Only an F-type spectrum is observed for the nonporous sample RW0, while SF-type spectra are observed for the two porous samples RW12 and RW12-SO_3^-. In the porous sample RW12, approximately 30% of the spin probes are immobilized with a rotational correlation time $\tau_2 = 13$ ns. In RW12-SO_3^- with sulfonated pore surface, the

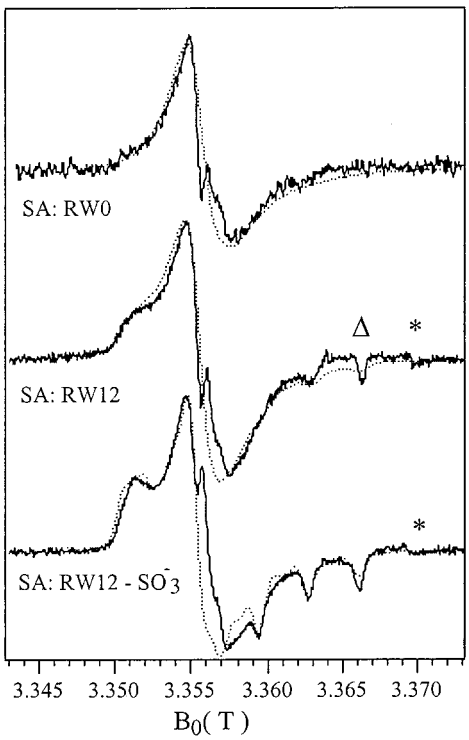

Figure 7. Effect of the presence and functionalization of pores on the ESR spectra of the SA spin probe. The superimposed dotted lines are the theoretical line shapes being expressed as a weighted sum of two components: one F-component ($\tau_2 = 1.6$ ns, $\epsilon_0 = 60°$) and one S-component ($\epsilon_0 = 60°$). The weight and the correlation time of the S-component are $w_s = 0.0$ for the nonporous sample (RW0), $w_s = 0.3$ and $\tau_2 = 13$ ns for the sample with unfunctionalized pores (RW12), and $w_s = 0.6$ and $\tau_2 = 26$ ns for the sample with pores functionalized by sulfonate groups (RW12-SO_3^-). The magnetic parameters for SA are $g_x = 2.0098$, $g_y = 2.0070$, $g_z = 2.0028$ and $A_x = 19.61$ MHz, $A_y = 14.01$ MHz, $A_z = 92.79$ MHz. The narrow peaks marked by triangles and asterisks are signals due to E_1' centers in the silica glass of the sample tubes and manganese impurities, respectively.

fraction of immobilized spin probes (60%) is higher than for the unfunctionalized pores, and their rotational correlation is longer ($\tau_2 = 26$ ns). Functionalization with hydroxyl groups does not have such an effect; i.e., the spectra of SA in RW12 and RW12-OH (not shown) are virtually the same (Table 2).

These effects cannot be solely due to the size and molecular shape of the probe, as size and shape are almost the same as for the ME probe. The ability of SA to discriminate between nonporous and porous samples must thus be attributed to the presence of a strongly polar headgroup. Furthermore, the slow fraction of the SA probes must be localized close to the pore surface, as it senses the sulfonate groups. In contrast, the fast fraction resides in the bulk, as its mobility is not influenced by the presence and functionalization of the pores.

This behavior finds a natural explanation in a structural memory effect. During the loading of the resin with spin probes and during washing, the pores are filled with the polar solvent. The surfactant spin probe may thus recognize the reverse micelle structure imposed by the templating and may insert into this structure at those sites where the AOT surfactant molecules were localized during synthesis. Its localization would then be analogous to the localization of the polymerizable surfactants shown in the bottom of Figure 1. The effect is reinforced by the presence of other ionic groups at the pore surface. Such a memory for the reverse micelle structure explains that a probe with a size of only about 1 nm is sensitive to the presence of pores with an average size of about 10 nm. Note also that the targeting of the pore surface by the SA spin probes depends on a subtle balance between solvent and polymer polarity, as it fails in methanol suspensions of the resin and works in dichloromethane solutions.

Conclusions

Various ESR spin probes can be used to characterize different structural aspects of porous polymer resins. Moreover, their spectra indicate how the pores can be filled or washed selectively. Unpolar spin probes of a sufficiently large size are mainly found in rigid, densely cross-linked regions of the resin if the loading is performed in methanolic suspensions. The subsequent washing with the less polar solvent dichloromethane induces a distribution of such unpolar probes between densely cross-linked and less cross-linked regions. Unpolar spin probes are insensitive to the presence and functionalization of pores.

In contrast, a fraction of the surfactant probe SA is trapped close to the pore surface when the weakly polar solvent dichloromethane is used. This fraction can be increased and becomes dominant by functionalization of the pore surface with sulfonate groups. Esterification of the surfactant headgroup of the spin probe effectively eliminates this sensitivity to the presence and functionalization of the pores. This preference of a surfactant headgroup for the surface of pores created by imprinting with reverse micelles can be considered as a structural memory effect, governed by size, shape, and amphiphilic character of the molecule. The detection of such subtle differences in site selectivity of probe molecules or additives by high-field EPR may also be of interest for the study of heterogeneous polymeric materials and of the principles that govern self-assembly of soft matter by supramolecular interactions. Further work along these lines is now in progress.

Acknowledgment. The authors thank ESTAC and NSERC of Canada for the financial support of this work. X.X.Z. thanks the Alexander von Humboldt Stiftung for a fellowship, and D.L. thanks the Max-Planck-Gesellschaft for the financial support during their sabbatical stays in the Max-Planck-Institut für Polymerforschung.

References and Notes

(1) Shea, K. J.; Spivak, D. A.; Sellergren, B. *J. Am. Chem. Soc.* **1993**, *115*, 3368.
(2) Smigol, V.; Svec, F.; Fréchet, J. M. J. *Macromolecules* **1993**, *26*, 5615.
(3) Vlatakis, G.; Andersson, L. I.; Müller, R.; Mosbach, K. *Nature (London)* **1993**, *361*, 645.
(4) Andersson, L. I.; Müller, R.; Mosbach, K. *Macromol. Rapid Commun.* **1996**, *17*, 65.
(5) Dabulis, K.; Klibanov, A. M. *Biotechnol. Bioeng.* **1992**, *39*, 176.
(6) Kempe, M.; Glad, M.; Mosbach, K. *J. Mol. Recognit.* **1995**, *8*, 35.
(7) Mathew, J.; Buchardt, O. *Bioconjugate Chem.* **1995**, *6*, 524.
(8) Wulff, G. *Angew. Chem., Int. Ed. Engl.* **1995**, *34*, 1812.
(9) Steinke, J.; Sherrington, D. C.; Dunkin, I. R. *Adv. Polym. Sci.* **1995**, *123*, 81.
(10) Mosbach, K.; Ramström, O. *Bio/Technology* **1996**, *14*, 163.
(11) Menger, F. M.; Tsuno, T.; Hammond, G. S. *J. Am. Chem. Soc.* **1990**, *112*, 1263.
(12) Menger, F. M.; Tsuno, T. *J. Am. Chem. Soc.* **1990**, *112*, 6723.

(13) Zhu, X. X.; Banana, K.; Yen, R. *Macromolecules* **1997**, *30*, 3031.
(14) Zhu, X. X.; Banana, K.; Liu, H. Y.; Krause, M.; Yang, M. *Macromolecules* **1999**, *32*, 277.
(15) Ousalem, M.; Zhu, X. X.; Hradil, J. *J. Chromatogr. A* **2000**, *903*, 13.
(16) *Electron Spin Relaxation in Liquids;* Muus, L. T., Atkins, P. W., Eds.; Plenum: New York, 1972.
(17) *Spin Labeling: Theory and Applications;* Berliner, L. J., Ed.; Academic Press: New York, 1976.
(18) Boyer, R. F., Keinath, S. E., Eds.; *Molecular Motion in Polymers by ESR;* Hanwood: Chur, 1980.
(19) *Biological Magnetic Resonance;* Berliner, L. J., Reuben, J., Eds.; Plenum: New York, 1989; Vol. 8.
(20) Weil, J. A.; Bolton, J. R.; Wertz, J. E. *Electron Paramagnetic Resonance*; Wiley: New York, 1994.
(21) *Structure and Transport Properties in Organized Polymeric Materials;* Chiellini, E., Giordano, M., Leporini, D., Eds.; World Scientific: Singapore, 1997.
(22) Cameron, G. G. In *Developments in Polymer Characterization*; Booth, C., Price, C., Eds.; Applied Sci. Pub.: London, 1987.
(23) Wasserman, A. M.; Khazanovich, T. N. In *Polymer Yearbook*; Pethrick, R. A., Ed.; Harwood Acad. Publ.: New York, 1995.
(24) Hommel, H. *Adv. Colloid Interface Sci.* **1995**, *54*, 209.
(25) Miller, W. G. In *Spin Labeling II: Theory and Applications;* Berliner, L. J., Ed.; Academic Press: New York, 1979.
(26) Schädler, V.; Franck, A.; Wiesner, U.; Spiess, H. W. *Macromolecules* **1997**, *30*, 3832.
(27) Baumgart, T.; Cramer, S.; Jahr, T.; Veniaminov, A.; Adams, J.; Fuhrmann, J.; Jeschke, G.; Wiesner, U.; Spiess, H. W.; Bartsch, E.; Sillescu, H. *Macromol. Symp.* **2000**, *151*, 451.
(28) Cramer, S. E.; Jeschke, G.; Spiess, H. W. *Macromol. Chem. Phys.* **2002**, *203*, 182; **2002**, *203*, 192.
(29) Pace, M. D.; Snow, A. W. *Macromolecules* **1995**, *28*, 5300.
(30) Faetti, M.; Giordano, M.; Pardi, L.; Leporini, D. *Macromolecules* **1999**, *32*, 1876.
(31) Dimeglio, J. M.; Baglioni, P. *J. Phys. Chem.* **1994**, *98*, 5478.
(32) Ottaviani, M. F.; Andechaga, P.; Turro, N. J.; Tomaglia, D. A. *J. Phys. Chem. B* **1997**, *101*, 6057.
(33) Zhou, L.; Schlick, S. *Polymer* **2000**, *41*, 4679.
(34) Szajdzinskapietek, E.; Pilar, J.; Schlick, S. *J. Phys. Chem.* **1995**, *99*, 313.
(35) *Advanced EPR*; Hoff, A. J., Ed.; Elsevier: Amsterdam, 1989.
(36) Budil, D. E.; Earle, K. A.; Freed, J. H. *J. Phys. Chem.* **1993**, *97*, 1294.
(37) Cramer, S.; Bauer, C.; Jeschke, G.; Spiess, H. W. *Appl. Magn. Reson.*, in press.
(38) Giordano, M.; Grigolini, P.; Leporini, D.; Marin, P. *Adv. Chem. Phys.* **1985**, *62*, 321.
(39) Andreozzi, L.; Giordano, M.; Leporini, D. In *Structure and Transport Properties in Organized Polymeric Materials*; Chiellini, E., Giordano, M., Leporini, D., Eds.; World Scientific: Singapore, 1997.
(40) Schneider, D. J.; Freed, J. H. In *Biological Magnetic Resonance;* Berliner, L. J., Reuben, J., Eds.; Plenum: New York, 1989; Vol. 8.
(41) Alessi, L.; Andreozzi, L.; Faetti, M.; Leporini, D. *J. Chem. Phys.* **2001**, *114*, 3631.

MA011861A